An Experimental and Theoretical Investigation of Ion−Molecule Reactions Involving Methyl Halide Radical Cations with Methyl Halides

Linda S. Nichols, Michael L. McKee,* and Andreas J. Illies*

Contribution from the Department of Chemistry, Auburn University, Auburn, Alabama 36849-5312

Received October 20, 1997

Abstract: An experimental and computational study of ion−molecule association reactions of the methyl halides has been carried out. A two-center three-electron bonded species, $[CH_3X\therefore XCH_3]^{\bullet+}$, has been observed for I and Br. MS/MS metastable and collision-induced dissociation experiments provide strong support of the atomic connectivity for both species. Computationally, two $[C_2H_6Cl_2]^{\bullet+}$ structures have been found: the 2c-3e bonded dimer, $[CH_3Cl\therefore ClCH_3]^{\bullet+}$, and the ylide bound structure, $[CH_3Cl-H-ClCH_2]^{\bullet+}$. Both are supported by the MS/MS results which give evidence of the CH_2Cl^+, $CH_3Cl^{\bullet+}$, and CH_3ClH^+ fragment ions. The study of $[C_2H_6F_2]^{\bullet+}$ proved to be somewhat more complicated. Three $[C_2H_6F_2]^{\bullet+}$ structures were found computationally: the 2c-3e bonded dimer, $[CH_3F\therefore FCH_3]^{\bullet+}$, a dihydrogen bonded structure, $[FH_2CH-HCH_2F]^{\bullet+}$, and a hydrogen bonded structure, $[CH_3F-HCH_2F]^{\bullet+}$. The F−H bonded species was computed to be the most stable. Kinetic energy release distributions, KERDs, have been measured for all the metastable reaction products and compared with KERD models obtained by using statistical phase space theory. We report here the experimental and theoretical results and the theoretical potential energy surface for all four systems.

Introduction

Organic halides, which have been extensively used as refrigerants, propellants, pesticides, and solvents, are known environmental contaminants. The effect of chlorine and fluorine on ozone depletion has been widely studied; however, bromine has recently been shown to be 50 times more effective, on a per atom basis, than chlorine at destroying ozone.[1] Studies show that most of the methyl bromide released into the atmosphere is degraded in the troposphere and contributions to stratospheric bromine levels are small.[2] However, even in small amounts, bromine's effectiveness at destroying ozone makes it a significant environmental threat. Methyl iodide can also react with ozone, although its environmental impact is currently minimal. Most of the methyl iodide present in the atmosphere now is believed to be of marine origin; however, recent studies have proposed using methyl iodide as a replacement for methyl bromide as a soil fumigant.[3]

Our group has long been interested in the 2c-3e bonding in gas-phase ion−molecule association reactions and recently began studying the formation of these hemibonds in the methyl halide systems. Gas-phase bimolecular methyl halide ion−molecule reactions have been previously studied by others,[4−6] yet very few gas-phase studies of the 2c-3e bonding in methyl halides exist.[7−9] This type of bonding, however, has been the subject of solution studies[10−12] and numerous theoretical investigations.[7,13,14] Here we present a detailed study of the formation of 2c-3e bonded methyl halides in the gas phase.

2c-3e bonding can be illustrated by the molecular orbital diagram shown below.

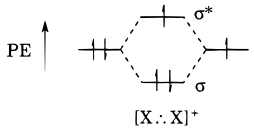

This type of bonding interaction was first studied by Linus Pauling in 1931.[15] The MO diagram predicts that, since the bond order is one-half, the 2c-3e bond should have a bond energy that is approximately one-half that of a normal 2c-2e bond. As a result of the lone electron occupying the σ^* antibonding orbital, this bond should also be much longer than a 2c-2e bond. These predictions have proved to be correct in prior studies of 2c-3e S∴S bonds.[16−18] Furthermore, Illies and

(1) Thomas, W. *Atmos. Environ.* **1996**, *30*, i and ii.
(2) Gennari, M.; Cignetti, A.; Gentile, I. A.; Vindrola, D. *Pestic. Sci.* **1995**, *45*, 221
(3) Sims, J. J.; Ohhr, H. D.; Grech, N. M. *Am. Nurseryman* **1997**, *185*, 64.
(4) Vaidyanathan, G.; Lyktey, M. Y. M.; Stry, J. J.; DeLeon, R. L.; Garvey, J. F. *J. Phys. Chem.* **1994**, *98*, 7475.
(5) Houriet, R.; Rolli, E.; Maquestiau, A.; Flammang, R.; Bouchoux, G. *Org. Mass. Spectrom.* **1987**, *22*, 770.
(6) Beauchamp, J. L.; Holtz, D.; Woodgate, S. D.; Patt, S. L. *J. Am. Chem. Soc.* **1972**, *94*, 2798.
(7) de Visser, S. P.; de Koning, L. J.; Nibbering, N. M. M. *J. Am. Chem. Soc.* Submitted for publication.
(8) Booze, J. A.; Baer, T. *J. Chem. Phys.* **1992**, *96*, 5541.
(9) Illies, A. J.; Livant, P. *J. Am. Chem. Soc.* **1991**, *113*, 1510.
(10) Maity, D. K.; Mohan, H. *Chem. Phys. Lett.* **1994**, *230*, 351.
(11) Asmus, K.-D.; Mohan, H. *J. Phys. Chem.* **1988**, *92*, 118.
(12) Shoute, L. C. T.; Neta, P. *J. Phys. Chem.* **1991**, *95*, 4411.
(13) Hess, A. B., Jr.; Zahradnik, R. *J. Am. Chem. Soc.* **1990**, *112*, 5731.
(14) Zahradnik, R. *Acc. Chem. Res.* **1995**, *28*, 306.
(15) Pauling, L. J. *J. Am. Chem. Soc.* **1931**, *53*, 3225.
(16) Knop, O.; Boyd, R. J.; Choi, S. C. *J. Am. Chem. Soc.* **1988**, *110*, 7299.
(17) Allen, F. H.; Kennard, O.; Watson, D. G.; Brammer, L.; Orpen, A. G.; Taylor, R. *J. Chem. Soc., Perkin Trans. 2* **1987**, *91*.
(18) Deng, Y.; Illies, A. J.; James, M. A.; McKee, M. L.; Peschke, M. *J. Am. Chem. Soc.* **1995**, *117*, 420.

S0002-7863(97)03644-5 CCC: $15.00
Published on Web 02/07/1998

Livant have previously estimated the enthalpy of reaction for the I∴I interaction in $[CH_3I\therefore ICH_3]^{\bullet+}$ to be within the 23−26 kcal/mol range.[9] This range is approximately 65% of a normal I−I 2c-2e interaction.

In studying the $[C_2H_6X_2]^{\bullet+}$ systems (X = I, Br, Cl, F), we hope to confirm the atomic connectivity of the methyl halide structures and to learn more about the nature of 2c-3e bonding. Furthermore, by using theoretical calculations and phase space modeling, we hope to learn more about the potential energy surface, PES, of each species studied.

Experimental Methods

MS/MS experiments on the $[C_2H_6X_2]^{\bullet+}$ dimers were carried out with a modified VG-ZAB 1F. These modifications have been described previously in the literature.[19,20] A collision cell has been added in the second field-free region and a variable-temperature ion source has also been incorporated. The scan control and signal detection were interfaced to a PC, the electrostatic analyzer, ESA, scan through a Cyber Research PC-166 16 bit D/A card, and signal detection through a Modern Instrumentation Technologies Inc. MTS 100 pulse preamplifier connected to a Cyber Research CYRCTM 05 timer/counter board. The scanning/data collection software was written in Microsoft Quick Basic for DOS.

The new ZAB ion source has been described in detail elsewhere.[19,20] It consists of a coaxial electron entrance/ion exit EI/CI source built from oxygen-free high-conductivity copper, beryllium/copper, stainless steel, glass, and ceramics. The source has a large width-to-length ratio of 3.4/1, which results in uniform electric fields over the entire volume covered by the ion exit slits. The source is heated and cooled by temperature-controlled air that passes through a heat-transfer tube that is silver-soldered to the source body.

The second field free region collision cell was placed just before the β-slit. Metastable scans were carried out in the second field-free region at a base pressure of 2×10^{-8} Torr with use of multiple scanning methods. Collision-induced dissociation, CID, spectra were also recorded with use of multiple scanning methods. Helium was used as a collision gas, and the parent peak intensity was reduced by 40%. Kinetic energy release distributions, KERD, were obtained from the metastable peaks shape by standard methods.[21]

Computational Methods

DFT Calculations. Calculations were performed by using the Gaussian 94 program system.[22] The geometry of each species was first optimized at the AM1 level and then used as the input for the density functional theory, DFT, calculations at the B3LYP/6-31+G(d) level of theory. The nature of the stationary points was checked by calculating vibrational frequencies. Due to their large size, a quasi-relativistic effective core potential developed by Bergner et al.[23] was used for the core electrons of bromine and iodine while the valence electrons were described with a 311/311/1 basis set contraction. The pseudopotential simulates the effects of the core shells while restricting quantum chemical treatment to the valence shell. DFT calculations have been shown to give a more accurate model of the energetics of reactions and bond dissociation than Hartree−Fock theory.[24] Furthermore, density functionals have been successful in reproducing known fundamental frequencies whereas HF, MP2, and QCISD results are systematically too large.[25] In addition, spin contamination does not seem to be as serious for DFT compared to HF theory.[26]

Unimolecular Kinetic Modeling. Calculations on KERDs were also performed by using statistical phase space modeling. The programs used for the phase space modeling were developed and supplied by Bowers and co-workers and have been used to describe systems with competing fragmentation pathways and to calculate the corresponding kinetic energy releases.[27] Parameters such as rotational constants, vibrational frequencies, and energies used in the phase space calculations were taken from the optimized DFT results. The programs include an ion-induced dipole attractive potential but not an ion−dipole potential. To compensate for this we used larger values[28] for the molecular polarizabilities.[29] The values used were obtained by scaling the ion-induced dipole plus ion−dipole potentials at distances of the appropriate bond distance plus 0.5 Å. The thermal ion−molecule collisions determine the collision complex energy and angular momentum distributions.[30] The energies used in modeling the KERDs are given in the text, and other molecular parameters used for the phase space modeling have been provided as Supporting Information.

Statistical phase space theory is similar to RRKM theory in that it is a microcanonical rate theory.[30] However, statistical phase space theory rigorously conserves energy and angular momentum in calculating the ability to pass over the transition state barrier. This theory has previously been shown to be successful in modeling KERDs for reactions which are statistical in nature.[21] At the core of this theory is the idea, or assumption, that the partitioning of energy among the reaction coordinate and all internal degrees of freedom at the transition state will remain statistical as the products are formed.[31] The ability to model the experimental KERDs allows us to examine the PES for each system in more detail.

Results and Discussion

MS/MS metastable and CID experiments give information on the structures of the species studied. CID fragmenting ions have greater internal energies than metastable ions, causing them to be short-lived; for this reason, CID fragmenting ions do not usually undergo extensive rearrangements. Metastable ions generally have sufficiently longer lifetimes, due to their lower internal energies, allowing for structural rearrangements to occur prior to fragmentation.[32,33] Hence, the metastable spectra are not as informative as CID spectra in deducing the atomic connectivity of ions.[34] Therefore, metastable experiments yield information on competing reactions and the PES of metastable species while CID experiments are used to provide direct evidence of the atomic connectivity of an ion.

(19) Illies, A. J.; Nichols, L. S.; James, M. A. *J. Am. Soc. Mass Spectrom.* **1997**, *8*, 605.
(20) James, M. A.; McKee, M. L.; Illies, A. J. *J. Am. Chem. Soc.* **1996**, *118*, 7836.
(21) Jarrold, M. F.; Illies, A. J.; Kirchner, N. J.; Wagner-Redecker, W.; Bowers, M. T.; Maudich, M. L.; Beauchamp, J. L. *J. Phys. Chem*. **1983**, *87*, 2213.
(22) Frisch, M. J.; Trucks, G. W.; Schlegel, H. B.; Gill, P. M. W.; Johnson, B. G.; Robb, M. A.; Checseman, J. R.; Kieth, T.; Petersson, G. A.; Montgomery, J. A.; Ragharachari, K.; Allaham, M. A.; Zakrzewski, V. G.; Ortiz, J. V.; Foresmar, J. B.; Cioslowski, J.; Stefanov, B. B.; Nanayakkara, A.; Challacombe, M.; Peng, C. Y.; Ayala, P. V.; Chen, W.; Martin, J.; Stewart, J. P.; Head-Gordon, M.; Gonzalez, C.; Pople, J. A. *Gaussian 94 (rev. B.1)*, Gaussian, Inc.: Pittsburgh, PA, 1995.
(23) Bergner, A.; Dolg, M.; Kuchle, W.; Stoll, H.; Preuss, H. *Mol. Phys.* **1993**, *80*, 1431.
(24) Ziegler, T. *Chem. Rev. (Washington, D.C.)* **1991**, *91*, 651.
(25) Johnson, B. G.; Gill, P. M. W.; Pople, J. A. *J. Chem. Phys*. **1993**, *98*, 5612.
(26) Baker, J.; Scheiner, A.; Andzelm, J. *Chem. Phys. Lett*. **1993**, *216*, 380.
(27) Carpenter, C. J.; Van Koppen, P. A. M.; Bowers, M. T. *J. Am. Chem. Soc*. **1995**, *117*, 10976.
(28) Illies, A. J.; Jarrold, M. F.; Bass, L. M.; Bowers, M. T. *J. Am. Chem. Soc.* **1983**, *105*, 5775.
(29) *CRC Handbook of Chemistry and Physics*: Lide, David R., Ed.; CRC Press: Inc.: Boca Raton, FL, 1994.
(30) Bass, L. M.; Cates, R. D.; Jarrold, M. F.; Kirchner, N. J.; Bowers, M. T. *J. Am. Chem. Soc*. **1983**, *105*, 7024.
(31) Hanratty, M. A.; Beauchamp, J. L.; Illies, A. J.; Van Koppen, P.; Bowers, M. T. *J. Am. Chem. Soc.* **1988**, *110*, 1.
(32) Jennings, K. R. *Int. J. Mass Spectrom. Ion Phys.* **1968**, *1*, 227.
(33) McLafferty, F. W.; Bente, P. F., III; Kornfeld, R.; Tsai, S. C.; Howe, I. *J. Am. Chem. Soc.* **1973**, *95*, 2120.
(34) Cooks, R. G.; Beynon, J. H.; Caprioli, R. M.; Lester, G. R. *Metastable Ions*; Elsevier Scientific Publishing Co.; Amsterdam, The Netherlands, 1973.

Table 1. Total Energies (hartrees) and Zero-Point Energies (kcal/mol)

species	PG	state	B3LYP/ 6-31+G* [a]	ZPE (NIF)[b]
$I^{\bullet}$		^2P	−11.38195	
CH_3I	C_{3v}	$^1A_1$	−51.32184	23.00 (0)
$CH_3I^{\bullet+}$	C_s	$^2A'$	−50.96372	21.51 (0)
$[(CH_3)_2I]^+$	C_{2v}	$^1A_1$	−90.92712	46.53 (0)
$[CH_3I\therefore ICH_3]^{\bullet+}$	C_{2h}	^2B_u	−102.33788	46.45 (1)
$[CH_3I\therefore ICH_3]^{\bullet+}$	C_2	^2B	−102.33926	46.51 (0)
$[CH_3I{-}CH_3{-}I]^{\bullet+}$	C_s	$^2A''$	−102.29698	46.19 (3)
$[CH_3I{-}CH_3{-}I]^{\bullet+}$ (TS)	C_1	^2A	−102.29763	(1)[c]
$Br^{\bullet}$		^2P	−13.34083	
CH_3Br	C_{3v}	$^1A_1$	−53.29979	23.34 (0)
$CH_3Br^{\bullet+}$	C_s	$^2A'$	−52.91017	21.25 (0)
$[(CH_3)_2Br]^+$	C_{2v}	$^1A_1$	−92.89541	47.15 (0)
$[CH_3Br\therefore BrCH_3]^{\bullet+}$	C_{2h}	^2B_u	−106.26726	47.01 (1)
$[CH_3Br\therefore BrCH_3]^{\bullet+}$	C_2	^2B	−106.28070	47.04 (0)
$[CH_3Br{-}CH_3{-}Br]^{\bullet+}$	C_s	$^2A'$	−106.22045	46.43 (3)
$[CH_3Br{-}CH_3{-}Br]^{\bullet+}$ (TS)	C_1	^2A	−106.22144	(1)[c]
$Cl^{\bullet}$		^2P	−460.13831	
CH_3Cl	C_{3v}	$^1A_1$	−500.11152	23.87 (0)
$CH_3Cl^{\bullet+}$	C_s	$^2A'$	−499.69731	20.60 (0)
$[(CH_3)_2Cl]^+$	C_2	^1A	−539.69577	48.16 (0)
$[CH_3Cl\therefore ClCH_3]^{\bullet+}$	C_{2h}	^2B_u	−999.86583	47.90 (1)
$[CH_3Cl\therefore ClCH_3]^{\bullet+}$	C_s	$^2A'$	−999.86586	47.93 (1)
$[CH_3Cl\therefore ClCH_3]^{\bullet+}$	C_2	^2B	−999.86595	47.94 (0)
$[CH_3Cl{-}H{-}ClCH_2]^{\bullet+}$	C_s	$^2A'$	−999.82236	43.72 (0)
$CH_2Cl^{\bullet}$	C_{2v}	$^2B_1$	−499.44251	14.27 (0)
CH_2Cl^+	C_{2v}	$^1A_1$	−499.11835	15.97 (0)
$CH_2ClH^{\bullet+}$	C_1	^2A	−499.66820	19.88 (0)
CH_3ClH^+	C_1	^2A	−500.35596	29.09 (0)
HCl	$C_{\infty v}$	$^1\Sigma_g$	−460.79800	4.60 (0)
$F^{\bullet}$		^2P	−99.73059	
CH_3F	C_{3v}	$^1A_1$	−139.75108	24.72 (0)
$CH_3F^{\bullet+}$	C_1	^2A	−139.28834	20.71 (0)
$[(CH_3)_2F]^+$	C_2	^1A	−179.31274	49.16 (0)
$[CH_3F\therefore FCH_3]^{\bullet+}$	C_{2h}	^2B_u	−279.08183	46.74 (0)
$[FH_2CH{-}HCH_2F]^{\bullet+}$	C_{2h}	^2B_u	−279.07587	45.50 (0)
$[CH_3F{-}H{-}CH_2F]^{\bullet+}$	C_s	$^2A'$	−279.09548	46.99 (0)
$CH_2F^{\bullet}$	C_s	$^2A'$	−139.07981	15.52 (0)
CH_2F^+	C_{2v}	$^1A_1$	−138.74285	17.00 (0)
CH_3FH^+	C_s	$^1A'$	−139.97857	30.39 (0)
HF	$C_{\infty v}$	$^1\Sigma_g$	−100.44337	5.63 (0)
$CH_3^{\bullet}$	D_{3h}	$^2A_2''$	−39.84203	18.69 (0)
CH_4	T_d	$^1A_1$	−40.52061	28.25 (0)

[a] I and Br calculations included the effective core potential from ref 23 and used a 311/311/1 basis set contraction basis set. [b] Zero-Point energy (kcal/mol) with number of imaginary frequencies in parentheses. [c] Optimizations converged to a transition state but vibrational frequencies were not calculated. Relative energies were computed by using the zero-point energy of the C_s symmetry structure.

Phase space calculations have been performed on the metastable products in order to model the measured KERDs and to clarify the fragmentation pathways for the PES. DFT calculations were performed in order to further elucidate the PES for each species studied. The absolute energies for the CH_3X neutrals, $CH_3X^{\bullet+}$ cations, and their association and reaction products were calculated at the B3LYP/6-31+G(d) level. The results are given in Table 1. Relative energies of all association products are given in Table 2.

$[CH_3I\therefore ICH_3]^{\bullet+}$ and $[CH_3{}^{81}Br\therefore {}^{81}BrCH_3]^{\bullet+}$. Two competing reactions were observed for the metastable decomposition of $[CH_3I\therefore ICH_3]^+$.

$$[CH_3I\therefore ICH_3]^{\bullet+} \rightarrow CH_3I^{\bullet+} + CH_3I \quad (1)$$

$$[CH_3I\therefore ICH_3]^{\bullet+} \rightarrow [(CH_3)_2I]^+ + I^{\bullet} \quad (2)$$

The most intense peak in the metastable product spectrum of $[CH_3I\therefore ICH_3]^{\bullet+}$, *m/z* 284 (Figure 1) is due to $CH_3I^{\bullet+}$, *m/z* 142, which occurs from direct cleavage of the 2c-3e bond, the weakest bond in the molecule. The second peak, $[(CH_3)_2I]^+$, *m/z* 157, originates from a fragmentation process that must involve structural rearrangement of the parent ion. This rearrangement product was also seen previously in ICR studies by Beauchamp et al.[6] These two peaks in the metastable spectrum show that there are two competing fragmentation pathways for $[CH_3I\therefore ICH_3]^{\bullet+}$.

Table 2. Relative Energies (kcal/mol) of Association Products[a]

species	energies (kcal/mol)
$[CH_3I\therefore ICH_3]^{\bullet+}$	−31.7
$[CH_3Br\therefore BrCH_3]^{\bullet+}$	−34.0
$[CH_3Cl\therefore ClCH_3]^{\bullet+}$	−32.0
$[H_2CCl{-}H{-}ClCH_3]^{\bullet+}$	−9.2
$[CH_3F\therefore FCH_3]^{\bullet+}$	−25.1
$[FH_2C{-}H{-}FCH_3]^{\bullet+}$	−35.1
$[FH_2CH{-}HCH_2F]^{\bullet+}$	−21.6

[a] Zero-point energy corrections have been included.

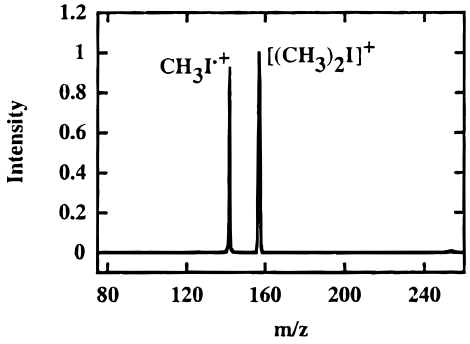

Figure 1. MS/MS metastable spectrum of $[CH_3I\therefore ICH_3]^{\bullet+}$.

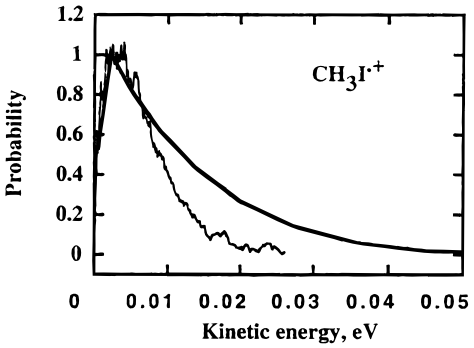

Figure 2. Metastable kinetic energy release distribution and kinetic modeling results for reaction 1. Phase space distributions are indicated by the solid continuous line.

Figure 2 shows the kinetic energy release distribution, KERD, obtained from the CH_3I^+ metastable peak. The KERD results in an average kinetic energy release, KER, of 6.5 meV. The small KER is consistent with direct fragmentation in a process that has a small or no reverse activation barrier. The distribution shape is also consistent with a direct fragmentation process since it peaks near 0 meV and its intensity falls to zero probability monotonically. The KERD for $[(CH_3)_2I]^+$ (Figure 3) extends over a much larger energy range than the KERD obtained for direct cleavage of the dimer—note that the *x*-axis scale in this plot is different than that in Figure 2. The average KER for $[(CH_3)_2I]^+$ is 51.5 meV compared to 6.5 meV for CH_3I^+. Both a large reverse activation barrier and a rearrangement forming lower energy products would contribute to a larger value for the average KER.[35] This indicates that a structural rearrangement is indeed occurring.

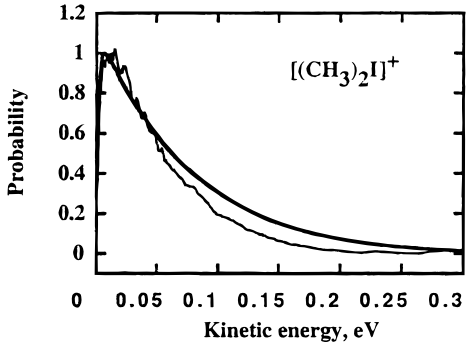

Figure 3. Metastable kinetic energy release distribution and kinetic modeling results for reaction 2. Phase space results are represented by the solid continuous line.

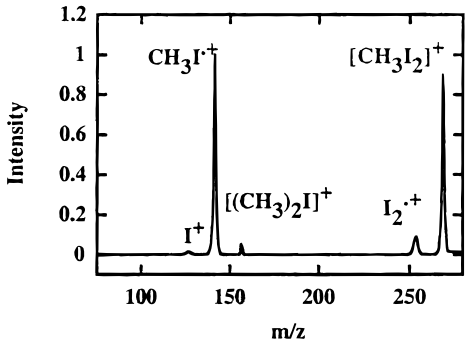

Figure 4. Collision-induced dissociation spectrum of $[CH_3I\therefore ICH_3]^{\bullet+}$.

The results of the phase space theory calculations modeling both competing pathways are also shown in Figures 2 and 3. In Figure 2, the agreement between the measured and calculated distributions for reaction 1 is tolerably good. This indicates that the KERD is statistical in nature. The modeled KERD in Figure 2 is often seen for a reaction involving a simple bond cleavage for which there is no barrier to the reverse association reaction.[31] The orbiting transition state used in calculating this surface resembles very loosely associated products.

Figure 3 shows the measured and calculated distributions for reaction 2. The KERD is broader than the previous KERD, Figure 2. In modeling this KERD, we used a tight transition state for the rearrangement and a loose orbiting transition state for the final step in the reaction. The use of phase space theory in modeling this type of reaction has been shown to be valid only if, after passing through the tight transition state, the trajectories remain statistical up to the orbiting transition state.[31]

The CID results for $[C_2H_6I_2]^{\bullet+}$ are presented in Figure 4. The most intense peak in this spectrum occurs at CH_3I^+, *m*/*z* 142, the product resulting from direct cleavage of the 2c-3e bond. The 2c-3e bond is the weakest bond in the ion. Therefore, one would expect the peak representing the species formed as a result of direct cleavage to be the most intense peak in the CID spectrum. $[CH_3I_2]^+$, *m*/*z* 269, the next most intense peak, results from breaking one I−C bond, which is a simple direct cleavage process. Peaks are also present at $I_2^{\bullet+}$, *m*/*z* 254; $[(CH_3)_2I]^+$, *m*/*z* 157; and I^+, *m*/*z* 127. The large difference in the $CH_3I^{\bullet+}$ and $[(CH_3)_2I]^+$ ratios in the metastable and CID spectra strongly support the conclusion that $CH_3I^{\bullet+}$ originates by direct bond cleavage while $[(CH_3)_2I]^+$ originates from a rearrangement process. The peaks at $I_2^{\bullet+}$, *m*/*z* 254 and I^+, *m*/*z* 127 are much less intense due to the number of bonds being broken.

(35) Hanratty, M. A.; Beauchamp, J. L.; Illies, A. J.; Van Koppen, P.; Bowers, M. T. *J. Am. Chem. Soc.* **1988**, *110*, 1.

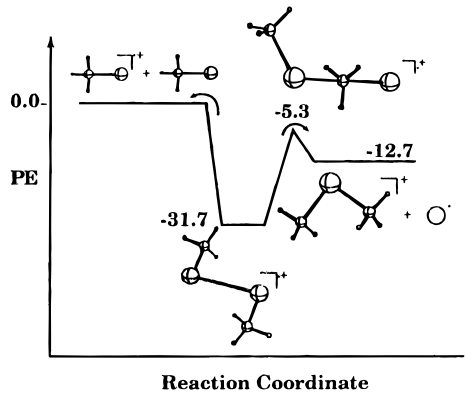

Figure 5. PES for $CH_3I^{\bullet+} + CH_3I$ undergoing an association reaction to form the 2c-3e bonded dimer before rearrangement to $[(CH_3)_2I]^+ + I^{\bullet}$. Energies are given in kcal/mol.

The theoretical potential energy surface for the reaction of $CH_3I^{\bullet+}$ with CH_3I is shown in Figure 5. The CH_3I neutral and $CH_3I^{\bullet+}$ monomers were chosen as the reference structures. The 2c-3e bonded dimer, formed from monomers (reaction 1), has C_2 symmetry and an I∴I binding energy of 31.7 kcal/mol, in reasonable agreement with an earlier I∴I bond energy estimate.[9] The C_{2h} structure, which is 0.9 kcal/mol higher in energy, is a transition state for rotation around the I∴I axis.

The $[CH_3I\therefore ICH_3]^{\bullet+}$ dimer undergoes a rearrangement via reaction 2 to form $[(CH_3)_2I]^+ + I^{\bullet}$. The migrating methyl group interacts with both iodines in the transition state with C−I distances of 2.81 and 2.62 Å. The transition vector is characterized as an asymmetric stretch involving the methyl carbon and both iodines. The transition state has C_1 symmetry while a stationary structure with C_s symmetry and three imaginary frequencies was located 0.4 kcal/mol higher in energy.

It can be seen (Figure 5) that the reaction forming $[(CH_3)_2I]^+$ has a significant reverse activation barrier of 7.4 kcal/mol, which results in a large KER, while direct cleavage of the 2c-3e bond involves essentially no reverse activation barrier, resulting in a small KER. The facts that (1) the rearrangement product is lower in energy than the reactants and (2) the possible involvement of a reverse activation barrier in the rearrangement process lead to more energy available for kinetic energy release in this channel. These observations parallel the experimental results shown in Figures 2 and 3.

$[CH_3Br\therefore BrCH_3]^{\bullet+}$ (*m*/*z* 192, the ^{81}Br containing species) behaves very similarly to the $[CH_3I\therefore ICH_3]^+$ system. Two competing reactions were also observed for this dimer.

$$[CH_3Br\therefore BrCH_3]^{\bullet+} \rightarrow CH_3Br^{\bullet+} + CH_3Br \qquad (3)$$

$$[CH_3Br\therefore BrCH_3]^{\bullet+} \rightarrow [(CH_3)_2Br]^+ + Br^{\bullet} \qquad (4)$$

The MS/MS results for the ion are shown in Figures 6 through 9.

Figure 6 shows the metastable product spectrum of $[CH_3Br\therefore BrCH_3]^{\bullet+}$. As was the case with $[CH_3I\therefore ICH_3]^{\bullet+}$, there are two peaks, $CH_3Br^{\bullet+}$, *m*/*z* 96, and $[(CH_3)_2Br]^+$, *m*/*z* 111. $CH_3Br^{\bullet+}$, *m*/*z* 96, results from a direct cleavage of the 2c-3e Br∴Br bond, the weakest bond in the ion, while $[(CH_3)_2Br]^+$, *m*/*z* 111, results from the rearrangement process shown in reaction 4. The KERD for the formation of $CH_3Br^{\bullet+}$, *m*/*z* 96 (Figure 7), results in an average KER of 5.5 meV. The KERD for $[(CH_3)_2Br]^+$, *m*/*z* 111, shown in Figure 8, is much broader than the KERD for $CH_3Br^{\bullet+}$ and results in a much larger

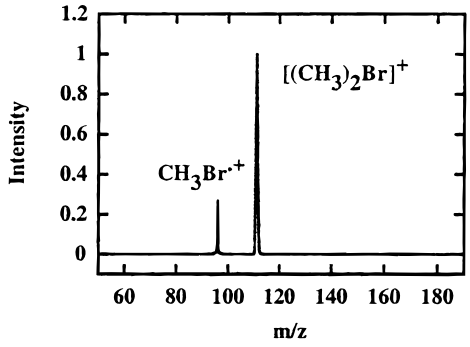

Figure 6. MS/MS metastable spectrum of $[CH_3{}^{81}Br\therefore{}^{81}BrCH_3]^{\bullet+}$.

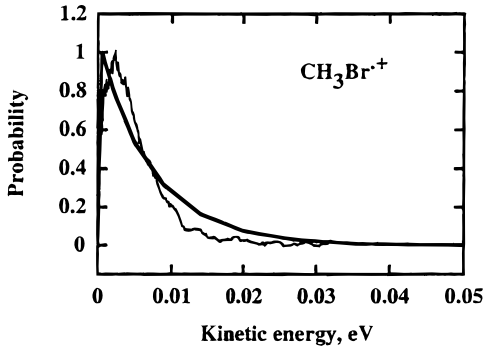

Figure 7. Metastable kinetic energy release distribution and kinetic modeling results for reaction 3. Phase space results are indicated by the solid continuous line.

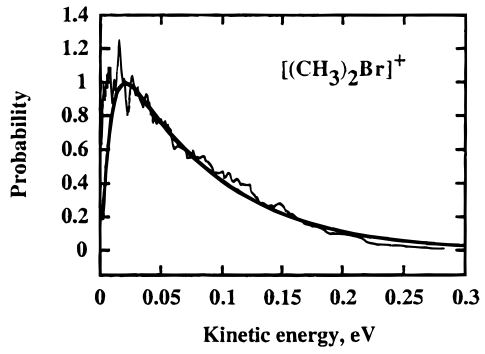

Figure 8. Metastable kinetic energy release distribution and kinetic modeling results for reaction 4. Phase space results are indicated by the solid continuous line.

average KER of 70.2 meV (note the different *x*-axis scale in Figures 7 and 8).

Figures 7 and 8 also summarize the phase space results for reactions 3 and 4, respectively. Since the $[CH_3Br\therefore BrCH_3]^{\bullet+}$ system was similar to the $[CH_3I\therefore ICH_3]^{\bullet+}$ system, we used the same assumptions to model the KERDs. The agreement between the calculated and the measured distributions is very good, indicating that the reactions are statistical in nature and exit through orbiting transition states.

The CID spectrum for the $[CH_3Br\therefore BrCH_3]^{\bullet+}$ (Figure 9) has four major peaks: $CH_3Br^{\bullet+}$, *m/z* 96; $[(CH_3)_2Br]^+$, *m/z* 111; $Br_2^{\bullet+}$, *m/z* 162; and $[CH_3Br_2]^+$, *m/z* 177. Cleavage of the 2c-3e bond results in $CH_3Br^{\bullet+}$, which is the strongest peak in the spectrum, while the product intensity due to the $[(CH_3)_2Br]^+$ rearrangement in the CID spectrum (Figure 9) is much lower. This further supports a direct fragmentation process for the formation of $CH_3Br^{\bullet+}$, *m/z* 96, and a rearrangement process for the formation of $[(CH_3)_2Br]^+$, *m/z* 111.

The theoretical PES for the $CH_3Br^{\bullet+}$ ion−molecule association reactions (Figure 10) is very similar to that for $CH_3I^{\bullet+}$ + CH_3I (Figure 5). Initially, the two reference monomers react to form the $[CH_3Br\therefore BrCH_3]^{\bullet+}$ dimer. The dimer has C_2 symmetry and lies 34.0 kcal/mol below the reference monomers. The dimer can then either cleave the 2c-3e bond or undergo an exothermic rearrangement (reaction 4) to form $[(CH_3)_2Br]^+$ + $Br^{\bullet}$ (13.9 kcal/mol below the reference monomers). The transition state for reaction 4 has C_1 symmetry and lies 5.4 kcal/mol below the reference monomers. As in the $[CH_3I\therefore ICH_3]^{\bullet+}$ system, a C_s stationary point with three imaginary frequencies was located 0.6 kcal/mol above the C_1 symmetry transition state. The resulting products, $[(CH_3)_2Br]^+ + Br^{\bullet}$, are lower in energy than the reactant monomers; this result again agrees with the larger average KER and broader KERD for the $[(CH_3)_2Br]^+$ product as compared to $CH_3Br^{\bullet+}$.

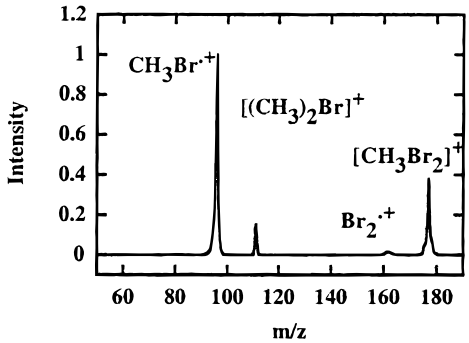

Figure 9. Collision-induced dissociation spectrum of $[CH_3{}^{81}Br\therefore{}^{81}BrCH_3]^{\bullet+}$.

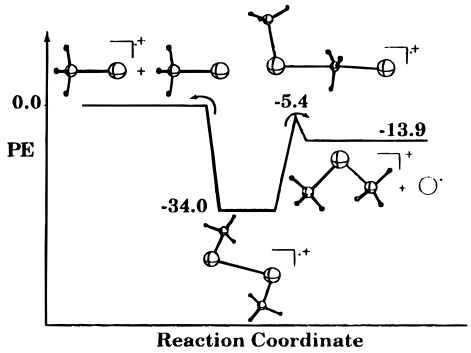

Figure 10. PES for $CH_3Br^{\bullet+}$ + CH_3Br undergoing an association reaction to form the 2c-3e bonded dimer before rearrangement to $[(CH_3)_2Br]^+ + Br^{\bullet}$. Energies are in kcal/mol.

$[C_2H_6{}^{35}Cl_2]^{\bullet+}$. Recently we learned of studies by Nibbering et al. who, with ab initio calculations, predicted the existence of two association products, $[CH_3Cl\therefore ClCH_3]^{\bullet+}$ and $[CH_2ClH\text{-}ClCH_3]^{\bullet+}$. They were able to form both ions by the ligand exchange reaction of Xe_2^+ with methyl chloride in an FT-ICR mass spectrometer.[7] Booze and Baer also formed the dimer ion in photoionization studies.[8]

Initially, our studies on $[C_2H_6Cl_2]^{\bullet+}$ (the ^{35}Cl-containing species) proved to be problematic. Three attempts to form the dimer were made. In the first attempt, we used neat CH_3Cl. The next attempt involved the use of N_2O as a bath gas. In both studies, there was a peak at *m/z* 100. However, the signal was so weak that MS/MS experiments for structure determination were inconclusive. A magnet scan, at a pressure of 1 Torr, on our highly modified DuPont mass spectrometer[36] showed that this peak did not increase significantly at lower temperatures which would promote clustering. Thus, there was no evidence to support the formation of a $[CH_3Cl\therefore ClCH_3]^{\bullet+}$

(36) Eckern, S.; Illies, A. J.; McKee, M. L.; Peschke, M. *J. Am. Chem. Soc.* **1995**, *115*, 12510.

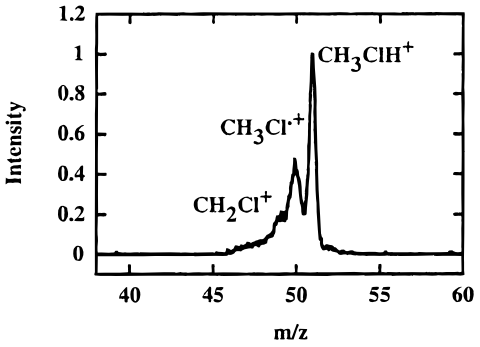

Figure 11. Collision-induced dissociation spectrum of $[C_2H_6{}^{35}Cl_2]^{\bullet+}$.

dimer in either system. Previous experiments on the $CH_3Cl^{\bullet+}$ ion−molecule association reactions by others failed to produce the dimer in the neat system at pressures up to 0.5 Torr.[37,38] Rolli et al. found that proton transfer (reaction 5)

$$[CH_3X]^{\bullet+} + CH_3X \rightarrow [CH_3XH]^+ + CH_2X^{\bullet} \qquad (5)$$

was endothermic in cases where X = Br, I and exothermic for X = Cl, F.[38] This proton-transfer reaction also occurred when X = Cl, F in the methyl halide studies by Beauchamp.[6]

Upon learning of the results by Nibbering et al.,[7] we attempted to form the association product by the Xe_2^+ ligand exchange reaction. Our CH_3Cl/Xe studies confirmed these findings. The intensity of the methyl chloride dimer radical cation was low and no metastable product ion could be observed; however, CID experiments, shown in Figure 11, could be carried out. Three peaks were observed: $CH_3Cl^{\bullet+}$ or $CH_2ClH^{\bullet+}$, *m*/*z* 50; CH_3ClH^+, *m*/*z* 51; and CH_2Cl^+, *m*/*z* 49. The presence of these products indicates that, much like the methyl fluoride system (see below), part of the observed $[C_2H_6Cl_2]^{\bullet+}$ association products at *m*/*z* 100 may not contain a 2c-3e bond. The following reactions help to explain the formation of each of the three products.

$$[CH_3Cl\therefore ClCH_3]^{\bullet+} \rightarrow CH_3Cl^{\bullet+} + CH_3Cl \qquad (6)$$

$$[CH_2ClH{-}ClCH_3]^{\bullet+} \rightarrow CH_2ClH^{\bullet+} + CH_3Cl \qquad (7)$$

$$[CH_2ClH{-}ClCH_3]^{\bullet+} \rightarrow CH_2Cl^{\bullet} + CH_3ClH^+ \qquad (8)$$

$$[CH_2ClH{-}ClCH_3]^{\bullet+} \rightarrow CH_2Cl^+ + CH_3{}^{\bullet} + HCl \qquad (9)$$

Hess et al. had computationally studied the $[C_2H_6Cl_2]^{\bullet+}$ system and had failed to find a minimum on the PES for $[C_2H_6Cl_2]^{\bullet+}$.[13] Our initial DFT studies resulted in the formation of $[CH_3ClH]^+$ and $CH_2Cl^{\bullet}$, the products of reaction 8. However, the recent ab initio calculations by Nibbering et al. resulted in two stable structures for the methyl chloride dimer radical cation, $[CH_3Cl\therefore ClCH_3]^{\bullet+}$ and $[CH_2ClH{-}ClCH_3]^{\bullet+}$.[7] We were also able to confirm the two structures for the $[C_2H_6Cl_2]^{\bullet+}$ species using DFT.

The PES calculated for this system (Figure 12) shows that the reference monomers, $CH_3Cl^{\bullet+}$ and CH_3Cl, undergo an association reaction to form the $[CH_3Cl\therefore ClCH_3]^{\bullet+}$ species. This C_2 symmetry species has a binding energy of 32.4 kcal/mol and fragments to form $CH_3Cl^{\bullet+}$ and CH_3Cl. The calculations also show that the monomer ylidium ion, $CH_2ClH^{\bullet+}$, can react with CH_3Cl to form $[CH_2ClH{-}ClCH_3]^{\bullet+}$. This ion was found

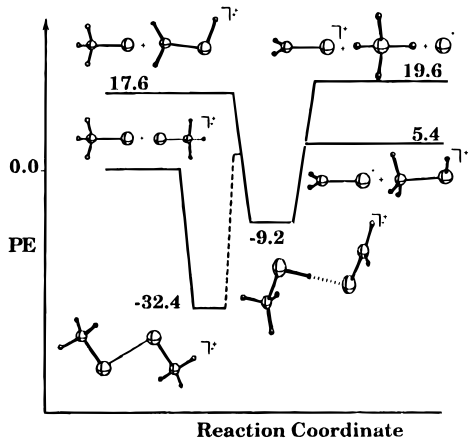

Figure 12. PES for $CH_3Cl^{\bullet+}$ + CH_3Cl undergoing an association reaction to form the 2c-3e bonded dimer. $CH_2ClH^{\bullet+}$ + CH_3Cl react to form the ylide bound structure. Energies are in kcal/mol.

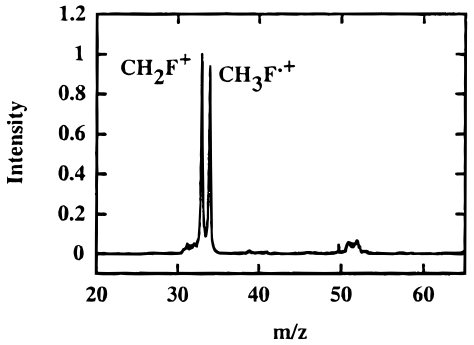

Figure 13. Collision-induced dissociation spectrum of $[C_2H_6F_2]^{\bullet+}$.

to have C_s symmetry and lie 9.2 kcal/mol below the reference monomers. Fragmentation of this species via reactions 7, 8, and 9 could result in the formation of $CH_2ClH^{\bullet+}$, CH_3ClH^+, and CH_2Cl^+, the ions observed in the CID spectrum. This association product alone could give rise to each of the peaks seen in the CID spectrum; however, the presence of $[CH_2ClH{-}ClCH_3]^{\bullet+}$ and $[CH_3Cl\therefore ClCH_3]^{\bullet+}$ at *m*/*z* 100 cannot be ruled out.

$[C_2H_6F_2]^{\bullet+}$. In previous studies on the methyl halides, Beauchamp noted that at pressures of 5×10^{-7} Torr, the only ions present were CH_2F^+, $CH_3F^{\bullet+}$, and CH_3^+. Only at increased pressures was the proton-transfer product, CH_3FH^+, seen.[6]

At even higher pressures, we observe the association reaction.

$$CH_3F^{\bullet+} + CH_3F \rightarrow [C_2H_6F_2]^{\bullet+} \qquad (10)$$

Our studies on $[C_2H_6F_2]^{\bullet+}$ were very different from those with methyl iodide or methyl bromide. Much like the $[C_2H_6Cl_2]^{\bullet+}$ results, the main beam was small and there was no detectable metastable; therefore, no KERs could be measured. The CID spectrum for $[C_2H_6F_2]^{\bullet+}$ is shown in Figure 13; it contains two peaks of almost equal intensity. $CH_3F^{\bullet+}$, *m*/*z* 34, is consistent with a 2c-3e bonded dimer; however, CH_2F^+, *m*/*z* 33, is also present. Formation of this product would require breaking two bonds in the 2c-3e bonded $[CH_3F\therefore FCH_3]^{\bullet+}$ dimer. On the basis of our previous studies, the cleavage of two bonds in the CID would result in a less intense peak than a peak resulting from the cleavage of one bond. The above observation indicates that the peak at CH_2F^+, *m*/*z* 33, should be less intense than the peak at $CH_3F^{\bullet+}$, *m*/*z* 34. However, this is not the case, the two peaks are of the same relative intensity. These results provide evidence for another association product.

(37) Lias, S. G.; Ausloos, P. *Ion−Molecule Reactions*; American Chemical Society: Washington, DC, 1975.

(38) Rolli, E.; Houriet, R.; Maquestiau, A.; Flammang, R.; Bouchoux, G. *Org. Mass. Spectrom.* **1987**, *22*, 770.

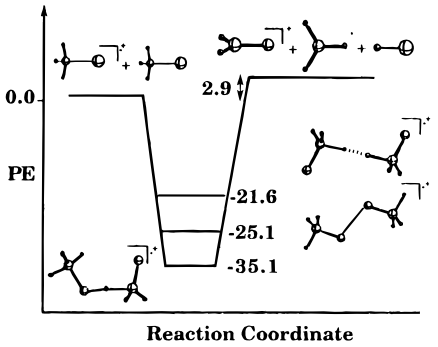

Figure 14. PES of $CH_3F^{\bullet+} + CH_3F$ forming three association products, a dihydrogen bonded structure, a 2c-3e bonded structure, and a hydrogen bonded structure. Energies are given in kcal/mol.

The potential energy surface for $CH_3F^{\bullet+} + CH_3F$ was computationally studied by Zahradnik[13,14] and reexamined in this study. The PES for this reaction (Figure 14) shows that the reference monomers, $CH_3F^{\bullet+}$ and CH_3F, can form three stable association products. Two of these were located by Zahradnik; however, using higher level calculations, we were able to locate a third, $[FH_2CH-FCH_3]^{\bullet+}$. The least stable of the products was $[FH_2CH-HCH_2F]^{\bullet+}$ (C_{2h} symmetry), which lies 21.6 kcal/mol below the reference monomers. The next most stable ion, $[CH_3F\therefore FCH_3]^{\bullet+}$, has C_{2h} symmetry and a bond energy of 25.1 kcal/mol. The most stable ion, $[FH_2CH-FCH_3]^{\bullet+}$, has C_s symmetry and lies 35.1 kcal/mol below the reference monomers. All of these products were stable minima on the surface with no imaginary frequencies.

All three of the association ions could be present in our experiment; however, $[FH_2CH-FCH_3]^{\bullet+}$ is the most consistent with the peaks shown in the CID spectrum (Figure 13). This ion would require the cleavage of the C−H bond to form the CH_2F^+ product and cleavage of the H−F bond to form the $CH_3F^{\bullet+}$ product. Since only one bond is broken in forming each of these products, the peak intensities for these two products are expected to be similar.

Conclusions

The experimental and computational results presented on the $[CH_3X\therefore XCH_3]^{\bullet+}$ radical cations support the presence of a 2c-3e bond for the cases where X = I or Br. The computational studies on these two systems also provide evidence of the 2c-3e bonded structure. The small average KERs for reactions 1 and 3 are consistent with a statistical unimolecular process with a small or no reverse activation barrier. The larger average KERs obtained for reactions 2 and 4 indicate that a rearrangement process occurs. Each of these mechanisms is supported by computational evidence.

The MS/MS CID experiments for the $[C_2H_6Cl_2]^{\bullet+}$ and $[C_2H_6F_2]^{\bullet+}$ radical cations do not fully support the presence of a 2c-3e bond; instead, they give evidence of a different atomic connectivity. The $CH_3Cl^{\bullet+}$ studies indicate that both $[CH_3Cl\therefore ClCH_3]^{\bullet+}$ and $[CH_3Cl-H-ClCH_2]^{\bullet+}$ could be present at *m/z* 100; however, $[CH_3Cl-H-ClCH_2]^{\bullet+}$ alone could give rise to the observed CID spectrum. Computational work indicates that the $[FH_2CH-FCH_3]^{\bullet+}$ cation is the most stable association product in the $CH_3F^{\bullet+} + CH_3F$ reaction. This ion is also most consistent with the formation of the equally intense experimental products, CH_2F^+ and $CH_3F^{\bullet+}$.

The ability to model the experimental KERDs so closely with phase space theory indicates that the reaction processes studied are statistical in nature. The good agreement between theory and experiment further clarifies the PES for each species studied.

Acknowledgment. A.J.I. is grateful to BASF for the donation of the ZAB 1F (serial no. 120). L.S.N. acknowledges the USDE for a Graduate Assistance in Area of National Needs (GAANN) fellowship. We also thank the Alabama Supercomputer Network for providing computer time for this study and David Young for his help with the phase space calculations. In addition, we would like to express our deep and sincere appreciation to Petra A. M. van Koppen and Michael T. Bowers (University of California, Santa Barbara) and Susan T. Graul (Carnegie Mellon) for their assistance with the phase space programs.

Supporting Information Available: Tables containing input parameters including symmetry numbers, polarizabilities, rotational constants, and vibrational frequencies used in the phase space calculations (2 pages, print/PDF). See any current masthead page for ordering and Web access instructions.

JA973644O